Measuring the refractive index dispersion of (un)pigmented biological tissues by Jamin-Lebedeff interference microscopy

Stavenga, Doekele G.; Wilts, Bodo D.

Published in:
AIP Advances

DOI:
10.1063/1.5113485

Publication date:
2019

Measuring the refractive index dispersion of (un)pigmented biological tissues by Jamin-Lebedeff interference microscopy

Cite as: AIP Advances **9**, 085107 (2019); https://doi.org/10.1063/1.5113485
Submitted: 04 June 2019 . Accepted: 31 July 2019 . Published Online: 12 August 2019

Doekele G. Stavenga, and Bodo D. Wilts

Measuring the refractive index dispersion of (un)pigmented biological tissues by Jamin-Lebedeff interference microscopy

Cite as: AIP Advances 9, 085107 (2019); doi: 10.1063/1.5113485
Submitted: 4 June 2019 • Accepted: 31 July 2019 •
Published Online: 12 August 2019

Doekele G. Stavenga[1] and Bodo D. Wilts[2,a)]

AFFILIATIONS

[1]Computational Physics, Zernike Institute for Advanced Materials, University of Groningen, NL-9747 AG Groningen, The Netherlands
[2]Adolphe Merkle Institute, University of Fribourg, CH-1700 Fribourg, Switzerland

[a)]bodo.wilts@unifr.ch

ABSTRACT

Jamin-Lebedeff interference microscopy is a powerful technique for measuring the refractive index of microscopically-sized solid objects. This method was classically used for transparent objects immersed in various refractive-index matching media by applying light of a certain predesigned wavelength. In previous studies, we demonstrated that the Jamin-Lebedeff microscopy approach can also be utilized to determine the refractive index of pigmented media for a wide range of wavelengths across the visible spectrum. The theoretical basis of the extended method was however only precise for a single wavelength, dependent on the characteristics of the microscope setup. Using Jones calculus, we here present a complete theory of Jamin-Lebedeff interference microscopy that incorporates the wavelength-dependent correction factors of the half- and quarter-wave plates. We show that the method can indeed be used universally in that it allows the assessment of the refractive index dispersion of both unpigmented and pigmented microscopic media. We illustrate this on the case of the red-pigmented wing of the damselfly *Hetaerina americana* and find that very similar refractive indices are obtained whether or not the wave-plate correction factors are accounted for.

I. INTRODUCTION

Understanding the physical basis of object colors crucially relies on quantitative knowledge of the refractive index of the constituent materials. This not only holds for structurally colored tissue in animal displays, often consisting of regularly arranged structures made up of materials with different refractive indices, but also for scattering media with irregularly organized tissue, as scattering crucially depends on the material's refractive index.[1–5] Accurate knowledge of the refractive index of small biological objects has remained limited, however, due to the difficulty to perform refractive index measurements on microscopically-sized objects.

A sensitive method for measuring the refractive index of biological tissue is Jamin-Lebedeff interference microscopy. The instrument, essentially a Jamin interferometer, was adopted by Lebedeff to a transmission optical microscope.[6] By using a birefringent crystal, the incident light beam is split into two perpendicularly polarized, spatially separated beams, one of which propagates through the test object and the other, the reference beam, bypasses the object and propagates through a medium of known refractive index. A second birefringent crystal recombines the beams. With a half-wave plate in between the beam splitter and combiner, and an additional quarter-wave plate, the phase shift induced by the test object can be determined with a rotatable linear analyzer.[7–11] The Jamin-Lebedeff interference microscope was originally designed for measuring the refractive index of transparent, i.e. absorptionless, media at a single, fixed wavelength (usually λ = 546 nm; the mercury green line). To determine the wavelength-dependent refractive index (the dispersion) approximative procedures using Cauchy's formula have been devised.[12]

We measured the refractive index and dispersion of insect chitin and bird keratin in unpigmented butterfly scales and bird feathers.[13] We furthermore developed a formalism for applying Jamin-Lebedeff interference microscopy on pigmented tissue and investigated insect wings and wing scales and bird feathers that contained common biological pigments, such as melanin, ommochromes, and pterins.[5,14–17] In these studies, we assumed that the retardation of wave-plates were wavelength-independent, which may create erroneous results at wavelengths remote from the instrument's central wavelength where the retardation of the plates strongly deviates from that at the designed wavelength. Here, we critically review our approach for refractive index measurements across the entire visible wavelength range. We present an extensive theoretical basis that takes the wavelength-dependent limitations of the instrument into account and demonstrate that the Jamin-Lebedeff interference microscope can be used for measuring the complex refractive index at any given wavelength for micro-sized, pigmented media.

II. THE OPTICAL COMPONENTS OF A JAMIN-LEBEDEFF INTERFERENCE MICROSCOPE SETUP

A Jamin-Lebedeff interference microscopy setup consists of a number of carefully designed optical components (Fig. 1). A light beam, delivered via the condenser of the microscope, first passes a linear polarizer (P) and is subsequently divided and spatially separated by a birefringent beam splitter (S) into an extra-ordinary (a) and ordinary ray (b). A half-wave plate (H) then rotates the polarization of both beams by 90°. Ray a travels through the object

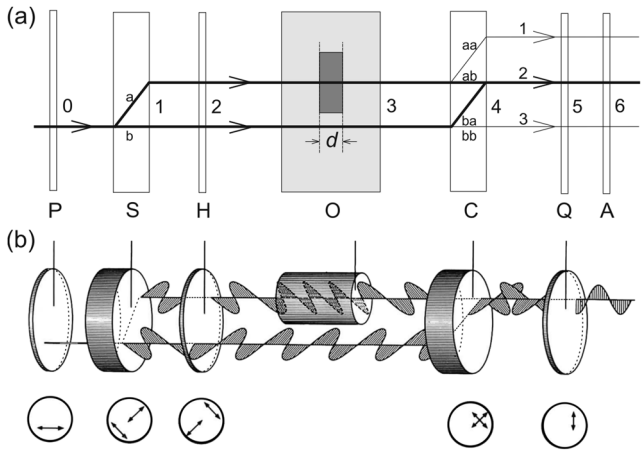

FIG. 1. Diagrams of the Jamin-Lebedeff interference microscope. a An object with thickness *d* is immersed in a reference medium (grey box). The extra-ordinary and ordinary beams are marked with the letters a and b, respectively. P, polarizer; S, beam splitter; H, half-wave plate; O, object; C, beam combiner; Q, quarter-wave plate; A, analyzer. Large numbers 0-6 indicate different levels of the light beams in the microscope; small numbers 1-3 indicate the three beams resulting after the beam combiner. b Propagation of the polarized beams through the microscope (from Ernst Leitz: Pol interference device according to Jamin/Lebedeff LINK).

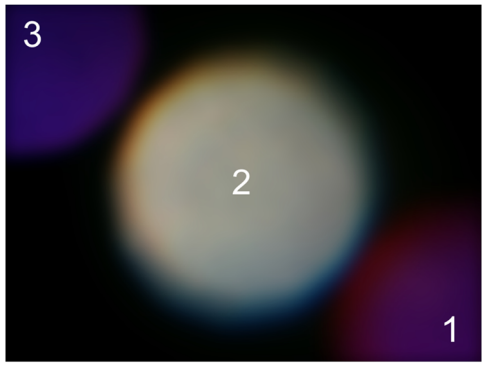

FIG. 2. Image of the three beams of the Jamin-Lebedeff interference microscope obtained with white light at level 6 of Figure 1 in the absence of an object and with analyzer angle α = 0°. The two purple-colored side beams (1 and 3) are due to the wavelength-dependent retardation of the wave plates present in the setup.

(O; Fig. 1, grey), which is immersed in a transparent fluid chosen so that it has approximately the refractive index of the object. Ray b proceeds through the immersion fluid, past the object. The two rays then enter a beam combiner (C) and subsequently pass a quarter-wave plate (Q; a Sénarmont compensator). The two rays combine into one ray for only one, ideal wavelength; at all other wavelengths three beams result due to the wavelength-dependence of the employed retarders (Fig. 2; beams 1-3 at level 4 of Fig. 1). The beams finally pass a rotatable linear polarizer, the analyzer (A). The half- and quarter-wave plates are oriented at 45° with respect to the polarization axes of the ordinary and extra-ordinary beams.

III. JONES FORMALISM FOR JAMIN-LEBEDEFF MICROSCOPY

The propagation of the light beams in a Jamin-Lebedeff microscope can be usefully treated with the Jones matrix formalism, where a vector describes the two components of a (linearly) polarized light beam and a matrix operation is equivalent to a polarization-changing optical element.[18] This approach has been previously applied to insect wings and bird feathers, but in these papers the wavelength-dependence of the half- and quarter-wave plates was neglected.[5,14–17] To specifically address this approximation will be the theme of the present paper.

We assume that the incident beam, after having passed the polarizer, has a unit power of light intensity at all wavelengths, and that the beam splitter divides the incident beam into two beams of equal intensity (a and b; Fig. 1). Taking a convenient coordinate system, we assume that the X-axis is parallel to the polarization of the extra-ordinary ray of the beam splitter, so that the Y-axis is parallel to the polarization of the ordinary ray.

IV. RETARDER CHARACTERISTICS

The half-wave plate H and the quarter-wave plate Q are retarders, for which the general Jones matrix is given by[18]

$$J(\phi,\theta)=\begin{bmatrix} e^{i\phi/2}\cos^2\theta+e^{-i\phi/2}\sin^2\theta & \left(e^{i\phi/2}-e^{-i\phi/2}\right)\sin(\theta)\cos(\theta) \\ \left(e^{i\phi/2}-e^{-i\phi/2}\right)\sin(\theta)\cos(\theta) & e^{i\phi/2}\sin^2\theta+e^{-i\phi/2}\cos^2\theta \end{bmatrix}=\begin{bmatrix} \cos(\phi/2)+i\sin(\phi/2)\cos(2\theta) & i\sin(\phi/2)\sin(2\theta) \\ i\sin(\phi/2)\sin(2\theta) & \cos(\phi/2)-i\sin(\phi/2)\cos(2\theta) \end{bmatrix} \tag{1}$$

with ϕ being the retardation angle and θ being the rotation angle. For the Jamin-Lebedeff setup presented here, the rotation angle for both H and Q is θ = -45° = -π/4, or, cos(2θ) = 0 and sin(2θ) = -1. It follows that

$$J\left(\phi,-\frac{\pi}{4}\right)=\begin{bmatrix} \cos(\phi/2) & -i\sin(\phi/2) \\ -i\sin(\phi/2) & \cos(\phi/2) \end{bmatrix} \tag{2}$$

A retarder with optical pathlength difference Δp between the ordinary and extra-ordinary ray introduces a phase difference $\phi = 2\pi\Delta p/\lambda = k\Delta p$, where λ is the wavelength and k the wavenumber of the applied illumination. At the wavelength where the pathlength difference is $\Delta p_h = \lambda_h/2$, the retarder acts as a half-wave plate (h), i.e., the retardation angle then is $\phi_h = \pi = 180°$, or,

$$J_h=-i\begin{bmatrix} 0 & 1 \\ 1 & 0 \end{bmatrix} \tag{3a}$$

At the wavelength where the pathlength difference is $\Delta p_q = \lambda_q/4$, the retarder acts as a quarter-wave plate (q), i.e., $\phi_q = \pi/2 = 90°$, or,

$$J_q=\frac{1}{2}\sqrt{2}\begin{bmatrix} 1 & -i \\ -i & 1 \end{bmatrix} \tag{3b}$$

(Note that for reasons of clarity we have chosen here a rotation angle θ different from the previous used value.[15])

The half- and quarter-wave plates of a Jamin-Lebedeff microscope are generally designed so that $\lambda_h = \lambda_q$, or, $\Delta p_h = 2\Delta p_q$ and $\phi_h = 2\phi_q$. In our previous studies, we assumed that Eqs. 3a,b are approximately valid for all wavelengths.[13,17] However, the retardation angles are wavelength-dependent due to dispersion of the birefringent material of the retarders. For a more general treatment we therefore we have to use Eq. 2, which then yields for the half-wave plate (H), with $\beta = \phi_h/2$,

$$J_h=\begin{bmatrix} \cos\beta & -i\sin\beta \\ -i\sin\beta & \cos\beta \end{bmatrix} \tag{4a}$$

and for the quarter-wave plate (Q), with $\gamma = \phi_q/2$,

$$J_q=\begin{bmatrix} \cos\gamma & -i\sin\gamma \\ -i\sin\gamma & \cos\gamma \end{bmatrix} \tag{4b}$$

The Jones matrix for the analyzer (A) positioned at rotation angle ρ is given by:[18]

$$J_A=\begin{bmatrix} \cos^2\rho & \sin\rho\cos\rho \\ \sin\rho\cos\rho & \sin^2\rho \end{bmatrix}=\begin{bmatrix} \cos\rho & 0 \\ \sin\rho & 0 \end{bmatrix}\begin{bmatrix} \cos\rho & \sin\rho \\ 0 & 0 \end{bmatrix} \tag{5}$$

V. LIGHT PROPAGATION INSIDE THE JAMIN-LEBEDEFF MICROSCOPE

The transmission axis of the linear polarizer (P) is oriented at 45° with respect to the X-axis, and hence, with unit power for the incident beam, the light beam after the polarizer is described by

$$\mathbf{E}_P=\frac{1}{2}\sqrt{2}\begin{pmatrix} 1 \\ 1 \end{pmatrix} \tag{6}$$

i.e., the intensity of the incident light beam, at level 0 (see Fig. 1 for level descriptions), is $I_0 = \mathbf{E}_P^*\mathbf{E}_P = 1$. At level 1, after the beam splitter (S), the extra-ordinary (a, Fig. 1) and ordinary (b, Fig. 1) rays are then

$$\mathbf{E}_{1a}=\frac{1}{2}\sqrt{2}\begin{pmatrix} 1 \\ 0 \end{pmatrix} \tag{7a}$$

and

$$\mathbf{E}_{1b}=\frac{1}{2}\sqrt{2}\begin{pmatrix} 0 \\ 1 \end{pmatrix} \tag{7b}$$

At level 2, after the half-wave plate (H), Eqs. 4a and 7 yield

$$\mathbf{E}_{2a}=J_h\mathbf{E}_{1a}=\frac{1}{2}\sqrt{2}\begin{pmatrix} \cos\beta \\ -i\sin\beta \end{pmatrix} \tag{8a}$$

and

$$\mathbf{E}_{2b}=J_h\mathbf{E}_{1b}=\frac{1}{2}\sqrt{2}\begin{pmatrix} -i\sin\beta \\ \cos\beta \end{pmatrix} \tag{8b}$$

The two light beams subsequently travel through a reference medium with an immersed object; beam a travels through the object and beam b through the reference medium only. At level 3, both beams will be phase shifted with respect to level 2, by δ_a and δ_b, respectively. Accordingly, the two beams are given by

$$\mathbf{E}_{3a}=\frac{1}{2}\sqrt{2}e^{i\delta_a}\begin{pmatrix} \cos\beta \\ -i\sin\beta \end{pmatrix} \tag{9a}$$

and

$$\mathbf{E}_{3b}=\frac{1}{2}\sqrt{2}e^{i\delta_b}\begin{pmatrix} -i\sin\beta \\ \cos\beta \end{pmatrix} \tag{9b}$$

At level 4, the beam combiner combines the beams, but at wavelengths outside the ideal wavelength in total three beams will emerge

$$\mathbf{E}_{41}=\mathbf{E}_{aa}=\frac{1}{2}\sqrt{2}e^{i\delta_a}\cos\beta\begin{pmatrix} 1 \\ 0 \end{pmatrix} \tag{10a}$$

$$\mathbf{E}_{42}=\mathbf{E}_{ab}+\mathbf{E}_{ba}=-\frac{1}{2}\sqrt{2}i\sin\beta\begin{pmatrix} e^{i\delta_b} \\ e^{i\delta_a} \end{pmatrix}=-\frac{1}{2}\sqrt{2}i\sin\beta e^{i\delta_b}\begin{pmatrix} 1 \\ e^{-i\delta} \end{pmatrix} \tag{10b}$$

$$\mathbf{E}_{43} = \mathbf{E}_{bb} = \frac{1}{2}\sqrt{2}e^{i\delta_b}\cos\beta\begin{pmatrix}0\\1\end{pmatrix} \tag{10c}$$

where the phase difference $\delta_b - \delta_a = \delta$ will be generally complex, with real (R) and imaginary (I) components δ_R and δ_I, or

$$\delta = \delta_R + i\delta_I \tag{11}$$

At level 5, after the quarter-wave plate,

$$\mathbf{E}_{51} = J_q\mathbf{E}_{41} = \tfrac{1}{2}\sqrt{2}e^{i\delta_a}\cos\beta\begin{pmatrix}\cos\gamma\\-i\sin\gamma\end{pmatrix} \tag{12a}$$

$$\mathbf{E}_{52} = J_q\mathbf{E}_{42} = -\frac{1}{2}\sqrt{2}ie^{i\delta_b}\sin\beta\begin{pmatrix}\cos\gamma - i\sin\gamma e^{-i\delta}\\-i\sin\gamma + \cos\gamma e^{-i\delta}\end{pmatrix} \tag{12b}$$

$$\mathbf{E}_{53} = J_q\mathbf{E}_{43} = \frac{1}{2}\sqrt{2}e^{i\delta_b}\cos\beta\begin{pmatrix}-i\sin\gamma\\\cos\gamma\end{pmatrix} \tag{12c}$$

so that at level 6, the light is split into three beams described by:

$$\mathbf{E}_{61} = J_A\mathbf{E}_{51} = \frac{1}{2}\sqrt{2}e^{i(\delta_b-\delta_R)}e^{\delta_I}\cos\beta(\cos\rho\cos\gamma - i\sin\rho\sin\gamma)\begin{pmatrix}\cos\rho\\\sin\rho\end{pmatrix} \tag{13a}$$

$$\mathbf{E}_{62} = J_A\mathbf{E}_{52} = -\frac{1}{2}\sqrt{2}ie^{i\delta_b}\sin\beta\Big[\cos\rho\Big(\cos\gamma - i\sin\gamma e^{-i\delta}\Big) + \sin\rho\Big(-i\sin\gamma + \cos\gamma e^{-i\delta}\Big)\Big]\begin{pmatrix}\cos\rho\\\sin\rho\end{pmatrix} \tag{13b}$$

$$\mathbf{E}_{63} = J_A\mathbf{E}_{53} = \frac{1}{2}\sqrt{2}e^{i\delta_b}\cos\beta(-i\cos\rho\sin\gamma + \sin\rho\cos\gamma)\begin{pmatrix}\cos\rho\\\sin\rho\end{pmatrix} \tag{13c}$$

VI. LIGHT INTENSITY AFTER THE ANALYZER

The intensities of the three light beams that leave the analyzer follow from Eq. 13 with $I = \mathbf{E}^*\mathbf{E}$. After some derivations (see Appendix A), it follows, with $t = e^{\delta_I}$, that

$$I_{61} = t^2\cos^2\beta\big[(\cos\rho\cos\gamma)^2 + (\sin\rho\sin\gamma)^2\big]/2 = \cos^2\beta[1 + \cos 2\gamma\cos 2\rho]/4 \tag{14a}$$

$$I_{62} = \sin^2\beta\big[\big(1+t^2\big) + \big(1-t^2\big)\cos 2\gamma\cos 2\rho + 2t(\cos\delta_R\sin 2\rho - \sin\delta_R\sin 2\gamma\cos 2\rho)\big] \tag{14b}$$

$$I_{63} = \cos^2\beta\big[(\sin\rho\cos\gamma)^2 + (\cos\rho\sin\gamma)^2\big]/2 = \cos^2\beta(1 - \cos 2\gamma\cos 2\rho)/4 \tag{14c}$$

Using $\beta = \phi_h/2$, $\gamma = \phi_q/2$, $\rho = \alpha + \pi/4$, and

$$c = \sin^2\beta = (1 - \cos 2\beta)/2 = (1 - \cos\phi_h)/2 \tag{15a}$$

$$t\cos\delta_R = a\cos(2\Delta\alpha) \tag{15b}$$

$$t\sin\delta_R\sin\phi_q - \big(1-t^2\big)\cos\phi_q/2 = a\sin(2\Delta\alpha) \tag{15c}$$

$$b = \big(1 + t^2 - 2a\big)/4 \tag{15d}$$

$$a = \Big\{\big[t\cos\delta_R\big]^2 + \big[t\sin\delta_R\sin\phi_q - \big(1-t^2\big)\cos\phi_q/2\big]^2\Big\}^{1/2} \tag{15e}$$

we obtain that the light intensities of the three beams after passing the analyzer are described by

$$I_{61} = t^2(1-c)(1 - \cos\phi_q\sin 2\alpha)/4 \tag{16a}$$

$$I_{62} = c\big\{2a\cos[2(a-\Delta\alpha)] + \big(1+t^2\big)\big\}/4 = c\big[a\cos^2(a-\Delta\alpha) + b\big] \tag{16b}$$

$$I_{63} = (1-c)(1 + \cos\phi_q\sin 2\alpha)/4 \tag{16c}$$

VII. MEASURING THE REFRACTIVE INDEX OF AN OBJECT AS A FUNCTION OF WAVELENGTH

The refractive index of an object can be determined by comparing the light intensity measured at a location within the object image and at a location outside that image as a function of wavelength λ. Yet, in experimental practice, the incident light beam at level 0, I_0, does not have unit power, or, the expressions for the intensity of the three light beams at level 6 have to be multiplied with $I_0 = I_0(\lambda)$. Accordingly, the light intensity in the object (o) area is $I_{62,o} = I_0\, I_{62}$, where I_{62} is given by Eq. 16b. Outside the object area, the phase difference $\delta = \delta_R = \delta_I = 0$, $a = 1$, $t = 1$, $b = 0$, and $\Delta\alpha = 0$, so that in the reference (r) area Eq. 16b yields

$$I_{62,r} = I_0 c\cos^2\alpha = I_0 c(1 + \cos 2\alpha)/2 \tag{17a}$$

or its peak value is

$$I^0_{62,r} = I_{62,r}(\alpha = 0) = I_0 c \tag{17b}$$

The ratio of the object and reference intensity is, with Eq. 16b,

$$I_{rel} = I_{62,o}/I^0_{62,r} = a\cos^2(\alpha - \Delta\alpha) + b \tag{17c}$$

By measuring $I_{62,o}$ and $I^0_{62,r}$ as a function of the rotation angle α at various wavelengths λ, the values of the parameters a and b as well as the phase shift $\Delta\alpha$ are experimentally obtained. We thus obtain the value of t, with Eq. 15d,

$$t = \sqrt{2a + 4b - 1} \tag{18a}$$

The real and imaginary parts of the phase difference $\delta = \delta_R + i\delta_I$ (Eq. 11) of beam a with respect to beam b (Fig. 1) are then derived with Eq. 15b as

$$\delta_R = \cos^{-1}[(a/t)\cos(2\Delta\alpha)] \tag{18b}$$

and with $t = e^{\delta_I}$

$$\delta_I = \ln(t) \tag{18c}$$

We note here that in the general, non-ideal situation only the quarter-wave plate affects the object's parameters, via ϕ_q (e.g. Eq. 15e). In other words, they are independent of the properties of the half-wave plate since the parameter c is divided out. If the

quarter-wave plate would have been ideal at all wavelengths, then $\phi_q = \pi/2$, or $a = t$ (Eq. 15e), $\delta_R = 2\Delta\alpha$ (Eq. 15b) and $b = (1 - a)^2/4$ (Eq. 15d); this case is treated in Ref. 15. Furthermore, for a fully transparent object, $a = t = 1$ and $b = 0$; the case treated in Ref. 13.

VIII. ESTIMATING THE THICKNESS OF THE OBJECT

For an object of thickness d (Fig. 1), the optical pathlength is given by

$$p = n_o d = (n_{oR} + i n_{oI}) d \tag{19a}$$

where n_o is the object's complex refractive index and n_{oR} and n_{oI} are its real and imaginary components. If the transparent reference medium has a refractive index n_r, the phase difference

$$\delta = k(n_r - n_o)d = k(n_r - n_{oR} - i n_{oI})d \tag{19b}$$

so that the real component of the phase difference becomes

$$\delta_R = kd(n_r - n_{oR}) = s(n_r - n_{oR}) \tag{20a}$$

which is a linear function of the refractive index of the reference fluid with slope

$$s = kd = 2\pi d/\lambda \tag{20b}$$

The thickness of the object follows from the slope of the linear fit by

$$d = s/k \tag{20c}$$

which must be the same for all experimental wavelengths λ.

The real part of the object's refractive index follows from Eq. 20a,

$$n_{oR} = n_r - \delta_R/(kd) = n_r - \delta_R/s \tag{20d}$$

and is equal to the refractive index of the immersion fluid when $\delta_R = 0$. The imaginary component of the phase difference is (Eqs. 11 and 19b)

$$\delta_I = -n_{oI} kd \tag{21a}$$

and the object's imaginary refractive index thus is, with Eqs. 18c, 20b,

$$n_{0I} = -\delta_I/(kd) = -\ln(t)/s \tag{21b}$$

The transmittance of a homogeneous object with thickness d and absorption coefficient κ is given by $T = \exp(-\kappa d)$, and the absorbance is $D(\lambda) = -\log_{10}[T(\lambda)]$. Since the absorption coefficient $\kappa = (4\pi/\lambda)n_{oI} = 2kn_{oI}$, it follows with Eq. 11 and 19b that $2\delta_I = -\kappa d$ and thus

$$t = \exp(\delta_I) = \exp(-\kappa d/2) = T^{1/2} \tag{21c}$$

so that the transmittance is, with Eq. 18a

$$T = t^2 = 2a + 4b - 1 \tag{21d}$$

Furthermore

$$n_{0I} = (0.5\ln 10)D/(kd) \tag{21e}$$

Not surprisingly, the imaginary part of the object's phase difference is intimately linked to the absorbance.

The above treatment shows that even without detailed knowledge of the retarders' dispersion properties, the refractive index of a microscopically-sized object can be reliably assessed as a function of wavelength by Jamin-Lebedeff microscopy for both transparent and absorbing media.

IX. THE CASE OF THE RED PIGMENTED WINGS OF THE DAMSELFLY HETAERINA AMERICANA

In a previous study, we investigated the optical properties of the wings of the damselfly *Hetaerina americana* and determined the refractive index dispersion by applying Jamin-Lebedeff microscopy, however, while neglecting possible imperfections due to the wave plates' dispersion.[15] For the measurements, we used a Zeiss Universal Microscope equipped with a Zeiss Pol-Int I 10x/0.22 objective and a Coolsnap ES monochrome camera (Photometrics, Tucson, AZ).

To assess the effects of the wavelength-dependent retardation of the wave plates, we reanalyzed the data with the formalism presented above. Fig. 3a presents an example measurement of a red wing piece immersed in a reference fluid with refractive index 1.55 (at 589 nm; due to dispersion the value slightly varies with the wavelength; Series A, Cargille Labs, Cedar Grove, NJ). The light intensities were measured as a function of the analyzer position and then divided by the maximum intensity measured in the reference area. Fig. 3a shows that the red wing part clearly exerts a considerable phase shift $\Delta\alpha$ as well as causes a strongly reduced amplitude a, due to the presence of an absorbing pigment.

We performed similar measurements to that of Fig. 3a on red wing pieces immersed in three different immersion fluids for a series of wavelengths. For each wavelength, we assessed the values of $\Delta\alpha$, a and b, and accordingly obtained the parameter t (Eq. 18a) and phase difference δ_R as a function of the immersion fluid's refractive index n_r (Eq. 18b), yielding the data points in Fig. 3b. The slope s of the linear functions (Eq. 20a,b) fitted to the data of each wavelength, together with the wavenumber k of the data points, yielded the thickness of the wing piece (Eq. 20c), with average $d = 2.5\ \mu$m (c.f. Figs. 3, 4 of Ref. 15).

The imaginary part of the refractive index, n_{oI}, subsequently followed from Eq. 21b for the three immersion fluids (Fig. 3c, JL). We independently derived the imaginary component from measurements of the wing absorbance with a microspectrophotometer, together with the wavenumber and the thickness (Eq. 21e; Fig. 3c, MSP). The n_{oI}-spectrum thus obtained corresponds well to the data extracted from the JL measurements.

For each wavelength, the real part of the refractive index, n_{oR}, followed from the zero-crossing of the linear fits of Fig. 3b (Eq. 20a), i.e. when $\delta_R = 0$ (Eq. 20d). Being obtained with the wave plate correction factors, these data are presented in Fig. 3d as 'corr' (the blue triangles). They only slightly differ from the 'uncorr' data (Fig. 3d, red circles with error bars), which were previously obtained with the procedure neglecting the wavelength dependence of the wave plates. In fact, the corrected data fall within the measurement errors of the uncorrected data,[15] indicating that the analysis of data with the simplified procedure previously applied is of similar validity as that with the more involved procedure outlined in the present paper. The reasons for this are discussed in Appendix B.

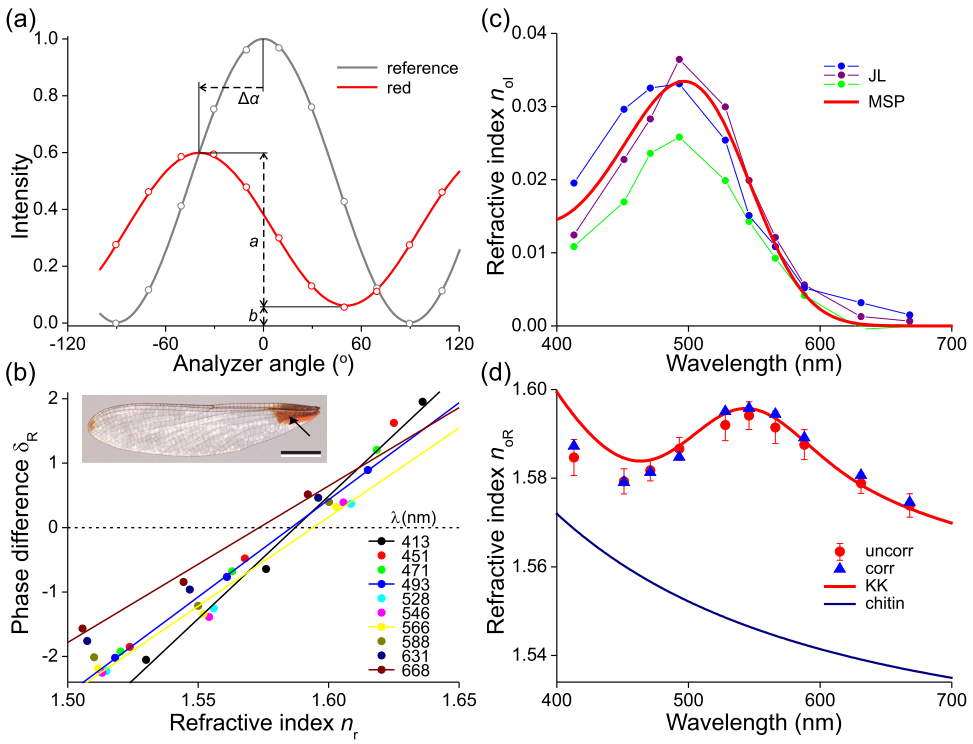

FIG. 3. Refractive index measurement of a wing of the damselfly *Hetaerina americana*. a Light intensity as a function of the analyzer angle in a red wing area (arrow in inset in b) compared to the reference area (wavelength 546 nm). The wing piece was immersed in a reference fluid with refractive index 1.55 at 589 nm. b Phase differences δ_R induced at a series of wavelengths λ by wing pieces in three reference fluids, with refractive indices n_r = 1.51, 1.55 and 1.60 at 589 nm. The data were calculated with Eq. 18a,b using the measured phase shift $\Delta\alpha$, amplitude *a* and background value *b* (inset, scale bar 5 mm). For each wavelength, the phase differences were fitted with a linear function (Eq. 20a); for clarity only 4 lines are shown. c Wavelength dependence of the imaginary part of the refractive index calculated with Eq. 21b for the three immersion cases (JL: Jamin-Lebedeff) together with the spectrum derived from absorbance measurements with a microspectrophotometer (MSP). d Wavelength dependence of the real part of the refractive index following from the zero crossings of the lines in b (corr; see Eq. 20d), together with the data derived with a simplified formalism (uncorr; from Ref. 15). The red curve (KK) was calculated with the Kramers-Kronig dispersion relation using the MSP spectrum extended into the UV, added to the refractive index spectrum of chitin (from Ref. 13; see text). The measurement data were taken from Ref. 15.

The n_{oR}-spectrum shows a clear anomalous dispersion in the 450-550 nm wavelength range, which is due to the strongly peaking imaginary refractive index in that wavelength region. The close relationship between the imaginary and real components of the refractive index are given by the Kramers-Kronig dispersion relations,[19] and we therefore calculated the contribution of the strongly blue-green absorbing, red transmitting pigment to the refractive index of chitin, the main wing material. To bring the measured data to match with the Kramers-Kronig data, we added the contribution of a hypothetical, strong-absorption band in the far-UV (Fig. 3d, KK; for details see Ref. 15). We thus confirm our previous finding that the red pigment considerably enhances the local refractive index of the damselfly wings.

X. EPILOGUE

The Jamin-Lebedeff interference microscopy method has received little attention in the recent decades, although several studies have shown that it allows the detailed measurement of the refractive index of microscopic bodies.[7–11] Exquisite instrumentation was produced and marketed by the major optical companies Zeiss as well as Leitz in the second half of the 20th century, but as the equipment has since gone out of production it can presently be only obtained second hand, unfortunately. One of the reasons may well have been that the measurements have become considered to be only suitable for a limited wavelength range and be restricted to transparent media. Furthermore, the manual execution and processing of the data may have been experienced to be somewhat cumbersome.

In the present paper we have demonstrated the validity of the method for transparent as well as pigmented media and for a broad wavelength range. Recently we have motorized the analyzer and equipped our microscope with a light source connected to a motorized monochromator. This enables a rapid, automatized analysis of the refractive index of interesting media, e.g. the wing scales of pierid butterflies.[5]

ACKNOWLEDGMENTS

This study was financially supported by the Air Force Office of Scientific Research/European Office of Aerospace Research and Development AFOSR/EOARD (grant FA9550-15-1-0068, to

D.G.S.), the National Centre of Competence in Research "Bio-Inspired Materials", and the Ambizione program of the Swiss National Science Foundation (168223, to B.D.W.). Bram van Zessen critically read the manuscript.

APPENDIX A: PROOF OF EQUATION 14b

Eq. 13b is

$$\begin{aligned}\mathbf{E}_{62} &= -\frac{1}{2}\sqrt{2}ie^{i\delta_b}\sin\beta\Big[\cos\rho\Big(\cos\gamma - i\sin\gamma e^{-i\delta}\Big) \\ &\quad + \sin\rho\Big(-i\sin\gamma + \cos\gamma e^{-i\delta}\Big)\Big]\begin{pmatrix}\cos\rho\\ \sin\rho\end{pmatrix} \\ &= -\frac{1}{2}\sqrt{2}ie^{i\delta_b}\sin\beta S\begin{pmatrix}\cos\rho\\ \sin\rho\end{pmatrix}\end{aligned} \tag{A1}$$

where

$$S = \cos\rho\Big(\cos\gamma - i\sin\gamma e^{-i\delta}\Big) + \sin\rho\Big(-i\sin\gamma + \cos\gamma e^{-i\delta}\Big) \tag{A2}$$

It follows with $t = e^{\delta_I}$ and $A = t\cos\delta_R$, $B = t\sin\delta_R$, $C = \cos\rho$, $D = \sin\rho$, $E = \cos\gamma$, $F = \sin\gamma$, that

$$\begin{aligned}S &= C[E - iF(A - iB)] + D[-iF + E(A - iB)] \\ &= CE - BCF + ADE - i(DF + ACF + BDE)\end{aligned} \tag{A3}$$

The intensity of light beam 62 is

$$I_{62} = \mathbf{E}_{62}^{*}\mathbf{E}_{62} = \sin^2\beta S^{*}S/2 \tag{A4}$$

Now

$$\begin{aligned}S^{*}S = |S|^2 &= (CE - BCF + ADE)^2 + (DF + ACF + BDE)^2 \\ &= (CE)^2 + (BCF)^2 + (ADE)^2 + (DF)^2 + (ACF)^2 + (BDE)^2 - 2BC^2EF + 2ACDE^2 - 2ABCDEF + 2ACDF^2 + 2BD^2EF + 2ABCDEF \\ &= \left(C^2E^2 + D^2F^2\right) + \left(A^2 + B^2\right)\left(C^2F^2 + D^2E^2\right) - 2BEF\left(C^2 - D^2\right) + 2ACD\left(E^2 + F^2\right) - 2BEF\left(C^2 - D^2\right) + 2ACD\left(E^2 + F^2\right)\end{aligned} \tag{A5}$$

Here $A^2 + B^2 = t^2$, $E^2 + F^2 = 1$, $2EF = \sin 2\gamma$ and $2CD = \sin 2\rho$. With $G = \cos 2\rho$ and $H = \cos 2\gamma$ it follows that $C^2 = (1 + G)/2$, $D^2 = (1 - G)/2$, $E^2 = (1 + H)/2$, $F^2 = (1 - H)/2$, $C^2 - D^2 = G$, $C^2E^2 + D^2F^2 = (1 + GH)/2$, and $(C^2F^2 + D^2E^2) = (1 - GH)/2$, so that

$$\begin{aligned}S^{*}S &= (1 + GH)/2 + t^2(1 - GH)/2 - 2BEFG + 2ACD = \left(1 + t^2\right)/2 + \left(1 - t^2\right)GH/2 + 2ACD - 2BEFG \\ &= \left(1 + t^2\right)/2 + \left(1 - t^2\right)\cos 2\rho\cos 2\gamma/2 + t(\cos\delta_R\sin 2\rho - \sin\delta_R\sin 2\gamma\cos 2\rho) \\ &= \left\{\left(1 + t^2\right) + \left[\left(1 - t^2\right)\cos 2\gamma - 2t\sin\delta_R\sin 2\gamma\right]\cos 2\rho + 2t\cos\delta_R\sin 2\rho\right\}2\end{aligned} \tag{A6}$$

With $\rho = \alpha + \pi/4$ and $2\gamma = \phi_q$ we derive

$$\begin{aligned}S^{*}S = \Big\{&\left(1 + t^2\right) + 2t\cos\delta_R\cos 2\alpha \\ &+ \left[2t\sin\delta_R\sin\phi_q - \left(1 - t^2\right)\cos\phi_q\right]\sin 2\alpha\Big\}/2\end{aligned} \tag{A7}$$

Using

$$t\cos\delta_R = a\cos(2\Delta\alpha) \tag{A8a}$$

and

$$t\sin\delta_R\sin\phi_q - \left(1 - t^2\right)\cos\phi_q/2 = a\sin(2\Delta\alpha) \tag{A8b}$$

we obtain

$$S^{*}S = \left(1 + t^2\right)/2 + a\cos 2(\alpha - \Delta\alpha) \tag{A9}$$

so that finally follows, with $c = \sin^2\beta$ and $b = [1 + t^2 - 2a]/4$,

$$\begin{aligned}I_{62} &= \sin^2\beta\left[2a\cos 2(\alpha - \Delta\alpha) + \left(1 + t^2\right)\right]/4 \\ &= c\left[a\cos^2(\alpha - \Delta\alpha) + b\right]\end{aligned} \tag{A10}$$

At each wavelength, ϕ_q has a certain value, dependent on the characteristics of the quarter-wave plate, which sets the values of $\sin\phi_q$ and $\cos\phi_q$ in Eq. A8b. The phase difference between the ordinary and extra-ordinary beam induced by the investigated object, $\delta = \delta_R + i\delta_I$, with real and imaginary components δ_R and δ_I (where $\delta_I = \ln t$), thus determines the values of the experimental parameters a and $\Delta\alpha$, via Eqs. A8a and A8b, as well as the value of the experimental parameter b, via Eq. 15b. (In the derivations, we have used the trigonometric expressions $\cos(2x) = 2\cos^2x - 1 = 1 - 2\sin^2x$, $\cos(x+\pi/2) = -\sin(x)$, and $\sin(x+\pi/2) = \cos(x)$.)

APPENDIX B: ASSESSMENT OF THE HALF-WAVE PLATE RETARDATION

According to the above derivation, it is not essential to know the wavelength dependence of the wave-plate retardation quantitatively, but it is nevertheless informative to assess this experimentally. To determine the parameter $c = (1 - \cos\phi_h)/2$ by which the half-wave plates affect the light intensities (Eq. 15a), we performed measurements without an object ($t = 1$) and with the quarter-wave plate taken out, i.e., we removed the Sénarmont compensator. Considering that then $\mathbf{E}_{6i} = J_A\mathbf{E}_{5i} = J_A\mathbf{E}_{4i}$ (i = 1-3), with $\delta = 0$, the intensities of the three beams become

$$I_{61} = (1 - c)(1 - \sin 2\alpha)/4 \tag{B1a}$$

$$I_{62} = c(1 + \cos 2\alpha)/2 \tag{B1b}$$

$$I_{63} = (1 - c)(1 + \sin 2\alpha)/4 \tag{B1c}$$

For analyzer angle $\alpha = 0$, Eq. B1 yields $I_{61} = I_{63} = (1 - c)/4$, $I_{62} = c$. By measuring the intensities of the side and central

beams and calculating their ratio, to again rule out the wavelength-dependence of the light beam intensity $I_0 = I_0(\lambda)$, we obtain

$$r_h = I_{61}/I_{62} = (1 - c)/(4c) \quad \text{(B2a)}$$

so that

$$c(\lambda) = 1/[4r_h(\lambda) + 1] \quad \text{(B2b)}$$

The wavelength-dependence of the retardation angle of the half-wave plate, ϕ_h, then is obtained with Eq. 15a

$$\phi_h(\lambda) = \cos^{-1}[1 - 2c(\lambda)] = \cos^{-1}\{1 - 2/[4r_h(\lambda) + 1]\} \quad \text{(B2c)}$$

Figure 4a show measurements of the half-wave plate ratio r_h (Eq. B2a). Implementing these data in Eq. B2c, the ϕ_h-values fitted with $\phi_h = P + Q\,\lambda^{-2}$ yield $P = 1.47$ and $Q = 4.71{\cdot}10^5$ nm^2, with λ in nm (Fig. 4a). Accordingly, a retardation angle of $\pi = 180°$ occurs at $\lambda = 531$ nm, somewhat below the green mercury line of 546 nm, the design wavelength of the Zeiss Jamin-Lebedeff system. This deviation appears to be unimportant when considering the very broad valley of the $r_h(\lambda)$-function in the green wavelength range, or, the half-wave plate correction factor c, resulting with Eq. 15a from the fit (Fig. 3b), is $c \approx 1$ in a wide wavelength range.

The retardation angle of the half-wave plate, $\phi_h = k\Delta p_h$, yields the pathlength difference between the ordinary and extra-ordinary rays, $\Delta p_h = d_h\,\Delta n$, where dh is the half-wave plate thickness and Δn the refractive index difference for the two rays. The wave plate is made of quartz, which has a birefringence described by.[20]

$$\Delta n = H + I\lambda^2/(\lambda^2 - G) + J\lambda^2/(\lambda^2 - L) \quad \text{(B3)}$$

where $H = 0.78890253{\cdot}10^{-3}$, $I = 8.04095323{\cdot}10^{-3}$, $G = 1.37254429{\cdot}10^{-2}$ μm^2, $J = 10.1933186{\cdot}10^{-3}$, $L = 64$ μm^2, λ in μm (Fig. 4a). By using this estimate of Δn, together with $\phi_h = 2\pi d_h \Delta n/\lambda$ and $r_h = (1 + \cos\phi_h)/[4(1 - \cos\phi_h)]$, the thickness of the half-wave plate can be calculated, yielding $d_h = 30$ μm. This plate causes a retardation angle of $\pi = 180°$ at $\lambda = 550$ nm.

The wavelength dependence of the retardation angle of the quarter-wave plate, made of the same material as the half-wave plate, follows from $\phi_q(\lambda) = \phi_h(\lambda)/2$. A quartz quarter-wave plate with thickness $d_q = 15$ μm thus causes a retardation angle of $\pi = 90°$ at $\lambda = 550$ nm. As expressed by Eq. 15c,e, the quarter-wave plate may play a crucial role in the Jamin-Lebedeff microscope measurements via the factors $\sin\phi_q$ and $\cos\phi_q$. Fig. 4c presents these factors where $\phi_q = (P + Q\,\lambda^{-2})/2$, with the values derived above, $P = 1.47$ and $Q = 4.71{\cdot}10^5$ nm^2.

The effect of the quarter-wave plate on the value of the amplitude a is illustrated in Fig. 4d for a few values of the transmittance parameter $t = \exp(\delta_I)$ and the real part of the phase difference δ_R. In a simplified view, where the wavelength dependence of the quarter-wave plate is neglected, the amplitude a equals t.[15] The calculations show that deviations from this idealized case exist in wavelength regions remote from the central wavelength (531 nm). These deviations increase when t decreases, i.e. when the absorbance of the measured object increases.

When the absorbance D is negligible, or the transmittance $T = t = 1$, then $a \approx t$ in a broad (visible) wavelength range (Fig. 4d, t =1.00), so that the classical Jamin-Lebedeff procedure as applied by Leertouwer et al.[13] is accurate. When absorption becomes noticeable, i.e. $t < 1$, then for $\delta_R = -0.5$ and $\delta_R = 0.5$ the values of a-t become opposite. Consequently, the slope of the linear fits, and thus the

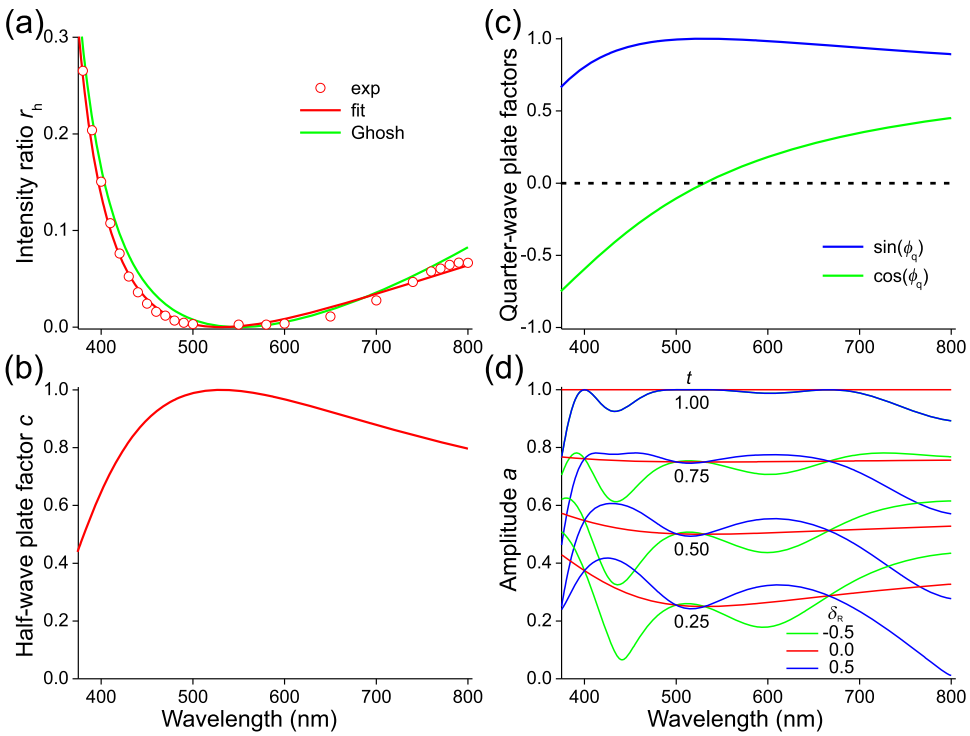

FIG. 4. Correction factors for the wavelength dependence of the half- and quarter-wave plates. a Experimentally determined intensity ratio r_h (Eq. B2a) fitted using the birefringence of a 30 μm thick quartz half-wave plate (Ref. 20 = Ghosh) and Eq. 15a. b The associated correction factor c (Eq. B2b). c Correction factors $\sin\phi_q$ and $\cos\phi_q$ of a 15 μm thick quartz quarter-wave plate. d Amplitude a for a few values of the parameter t and phase difference δ_R using the quarter-wave plate factors of c, calculated with Eq. 15e.

object's thickness will be underestimated, but the zero-crossings will not be severely affected. The example of the red wing of *Hetaerina americana* is a case in point. The maximal value of the imaginary part of the refractive index (0.033 at 500 nm, Fig. 3c) together with a thickness of 2.5 μm yields $t = 0.35$. At wavelengths deviating from the peak wavelength, t has higher values. Fig. 4d shows that with $t = 0.25$ the amplitude spectra for $\delta_R = -0.5$ and $\delta_R = 0.5$ are about symmetrical around the t-value; the situation for $t = 0.35$ will be similar. Due to the symmetry, as explained above, the n_{oR} values resulting from the zero-crossings of the linear fits will be little affected, so that the deviations between the 'corr' and 'uncorr' refractive indices are minor (Fig. 3d).

REFERENCES

[1] J. Schmitt, A. Knüttel, and R. Bonner, "Measurement of optical properties of biological tissues by low-coherence reflectometry," Appl. Opt. **32**, 6032–6042 (1993).

[2] R. O. Prum, "Anatomy, physics, and evolution of avian structural colors," in *Bird Coloration*, Vol. I, Mechanisms and Measurements, G. E. Hill and K. J. McGraw, eds. (Harvard University Press, Cambridge, Mass. 2006), pp. 295–353.

[3] S. Kinoshita, *Structural Colors in the Realm of Nature* (World Scientific, Singapore, 2008).

[4] S. L. Jacques, "Optical properties of biological tissues: A review," Phys. Med. Biol. **58**, R37 (2013).

[5] B. D. Wilts, B. Wijnen, H. L. Leertouwer, U. Steiner, and D. G. Stavenga, "Extreme refractive index wing scale beads containing dense pterin pigments cause the bright colors of pierid butterflies," Adv. Opt. Mater. **5**, 1600879 (2017).

[6] M. Françon, *Progress in Microscopy* (Pergamon Press, Oxford, 1961).

[7] J. M. Gillis and M. Wibo, "Accurate measurement of the thickness of ultrathin sections by interference microscopy," J. Cell Biol. **49**, 947–949 (1971).

[8] R. Laughlin, A. Marrer, C. Marcott, and R. Munyon, "An improved Sénarmont retardation analysis method," J. Microsc. **139**, 239–247 (1985).

[9] F. J. Schäfer and W. Kleemann, "High-precision refractive index measurements revealing order parameter fluctuations in $KMnF_3$ and NiO," J. Appl. Phys. **57**, 2606–2612 (1985).

[10] C. Ockleford, "A quantitative interference light microscope study of human first trimester chorionic villi," J. Microsc. **157**, 225–237 (1990).

[11] L. Donaldson, "Interference microscopy," in *Methods in Lignin Chemistry*, S. Y. Lin and C. W. Dence, eds. (Springer, Berlin 1992), pp. 122–132.

[12] J. Gahm, "Quantitative messungen mit der interferenzanordnung von Jamin-Lebedeff," Zeiss-Mitt **3**, 3–31 (1963).

[13] H. L. Leertouwer, B. D. Wilts, and D. G. Stavenga, "Refractive index and dispersion of butterfly scale chitin and bird feather keratin measured by interference microscopy," Opt. Express **19**, 24061–24066 (2011).

[14] D. G. Stavenga, H. L. Leertouwer, T. Hariyama, H. A. De Raedt, and B. D. Wilts, "Sexual dichromatism of the damselfly calopteryx japonica caused by a melanin-chitin multilayer in the male wing veins," PLoS One **7**, e49743 (2012).

[15] D. G. Stavenga, H. L. Leertouwer, and B. D. Wilts, "Quantifying the refractive index dispersion of a pigmented biological tissue using Jamin–Lebedeff interference microscopy," Light Sci. Appl. **2**, e100 (2013).

[16] B. D. Wilts, K. Michielsen, H. De Raedt, and D. G. Stavenga, "Sparkling feather reflections of a bird-of-paradise explained by finite-difference time-domain modeling," Proc. Natl. Acad. Sci. U. S. A. **111**, 4363–4368 (2014).

[17] D. G. Stavenga, H. L. Leertouwer, D. C. Osorio, and B. D. Wilts, "High refractive index of melanin in shiny occipital feathers of a bird of paradise," Light Sci. Appl. **4**, e243 (2015).

[18] D. H. Goldstein, *Polarized Light* (CRC Press, Boca Raton, 2010).

[19] V. Lucarini, J. J. Saarinen, K. Peiponen, and E. M. Vartiainen, *Kramers-Kronig Relations in Optical Materials Research* (Springer, Berlin, 2005).

[20] G. Ghosh, "Dispersion-equation coefficients for the refractive index and birefringence of calcite and quartz crystals," Opt. Commun. **163**, 95–102 (1999).